

NEAR-UV OBSERVATIONS OF CS29497-030: NEW CONSTRAINTS ON NEUTRON-CAPTURE NUCLEOSYNTHESIS PROCESSES

INESE I. IVANS^{2,3}, CHRISTOPHER SNEDEN⁴, ROBERTO GALLINO⁵,
JOHN J. COWAN⁶, AND GEORGE W. PRESTON⁷

Draft version August 28, 2018

ABSTRACT

Employing spectra obtained with the new Keck I HIRES near-UV sensitive detector, we have performed a comprehensive chemical composition analysis of the binary blue metal-poor star CS29497-030. Abundances for 29 elements and upper limits for an additional seven have been derived, concentrating on elements largely produced via neutron-capture nucleosynthesis. Included in our analysis are the two elements that define the termination point of the slow neutron-capture process, lead and bismuth. We determine an extremely high value of $[\text{Pb}/\text{Fe}] = +3.65 \pm 0.07$ ($\sigma = 0.13$) from three features, supporting the single-feature result obtained in previous studies. We detect Bi for the first time in a metal-poor star. Our derived Bi/Pb ratio is in accord with those predicted from the most recent FRANEC calculations of the slow neutron-capture process in low-mass AGB stars. We find that the neutron-capture elemental abundances of CS29497-030 are best explained by an AGB model that also includes very significant amounts of pre-enrichment of rapid neutron-capture process material in the protostellar cloud out of which the CS29497-030 binary system formed. Thus, CS29497-030 is both an $r+s$ and “extrinsic AGB” star. Furthermore, we find that the mass of the AGB model can be further constrained by the abundance of the light odd-element $[\text{Na}/\text{Fe}]$ which is sensitive to the neutron excess.¹

Subject headings: nuclear reactions, nucleosynthesis, abundances – stars: abundances – stars: Population II – stars: AGB – stars: binaries: spectroscopic – stars: individual (CS29497-030)

1. INTRODUCTION

The bulk of the “heavy elements”, those heavier than iron, are created by a combination of slow and rapid neutron-capture nucleosynthesis processes (s - and r -process) with each responsible for $\sim 50\%$ of the solar system isotopes. In the s -process, successive neutron captures occur over sufficiently long timescales to permit unstable nuclei to β -decay and, in principle, the isotopic distribution of the s -process can be calculated from knowledge of stellar and nuclear physics (e.g., Busso, Gallino, & Wasserburg 1999; Straniero, Gallino, & Cristallo 2005). Pb and Bi are the last stable elements along the s -process path. All isotopes heavier than Bi are unstable and α -decay to Pb and Bi (Clayton & Rassbach 1967). In the Sun, the elemental abundances of Pb and Bi consist of significantly different combinations of r - and s -process isotope contributions, with $r:s$ ratios for Pb and Bi of 21:79 and 65:35, respectively (Travaglio et al. 1999; Simmerer et al. 2004; and references therein). The

solar system chemical composition is the integrated result of many generations of stars, and depends upon the details of the formation history, initial mass functions, chemical yields, etc. The Pb and Bi abundances most useful for unravelling the sites and nuclear parameters associated with the s - and r -process correspond to those in extremely metal-poor stars, formed from material with few prior generations of nucleosynthetic processing.

In the last five years, dozens of low-metallicity stars with $[\text{Pb}/\text{Fe}] > 1$ have been discovered⁷ (e.g. Sivaranı et al. 2004; Barbuy et al. 2005; and references therein). Such large values of heavy s -process enhancements in low metallicity stars are thought to be the result of mass transfer in binary star systems where the initially more massive star underwent an asymptotic giant branch (AGB) evolutionary phase, and transferred material to the observed star. The Pb enhancements observed in metal-poor stars were predicted by Gallino et al. (1998) who noted that lower metallicity stars were expected to display increasingly higher abundances of heavier s -process elements relative to the abundances of lighter s -process elements. At lower metallicities, the number of neutrons captured per iron seed increases, allowing heavier elements to be produced in greater abundance. Pb enhancements have since been modelled by both phenomenological “classical” AGB models with parameterized neutron exposures and “stellar models” with stellar astrophysical constraints (e.g. Arlandini et al. 1999; De-

² Dept. of Astronomy, California Institute of Technology, Pasadena, CA 91125; iiii@astro.caltech.edu

³ Hubble Fellow.

⁴ Dept. of Astronomy, The University of Texas, Austin, TX 78712; chris@verdi.as.utexas.edu

⁵ Dipartimento di Fisica Generale, Universita’ di Torino, 10125 Torino, Italy; gallino@ph.unito.it

⁶ Dept. of Physics and Astronomy, University of Oklahoma, Norman, OK 73019; cowan@nhn.ou.edu

⁷ The Observatories of the Carnegie Institution of Washington, Pasadena, CA 91101; gwp@ociw.edu

¹The data presented herein were obtained at the W. M. Keck Observatory, which is operated as a scientific partnership among the California Institute of Technology, University of California, and NASA, and was made possible by the financial support of the W. M. Keck Foundation.

⁷ We adopt the usual spectroscopic notation that for elements A and B, $\log \epsilon(A) \equiv \log_{10}(N_A/N_H) + 12.0$, and $[A/B] \equiv \log_{10}(N_A/N_B)_* - \log_{10}(N_A/N_B)_\odot$. e.g., $[\text{Pb}/\text{Fe}] = 3 \Rightarrow (N_{\text{Pb}}/N_{\text{Fe}})_* = 1000 \times (N_{\text{Pb}}/N_{\text{Fe}})_\odot$. Also, metallicity is defined as the stellar $[\text{Fe}/\text{H}]$ value.

laude et al. 2004; and references therein).

Because Bi is the last stable element, knowledge of its abundance in metal-poor halo stars will help pin down the predictions of the abundances of heavier radioactive actinide elements such as Th and U (Kratz et al. 2004; Ratzel et al. 2004; and references therein). Thus, abundance determinations of this element will also benefit nuclear chronometer studies of the age of the Galaxy. With these multiple goals in mind, we observed the blue metal-poor star (BMP; Preston, Beers, & Schectman 1994), CS29497-030, a star which possesses the largest [Pb/Fe] abundance of any metal-poor star published to date (Snedden, Preston, & Cowan 2003 – SPC03; Van Eck et al. 2003, Sivarani et al. 2004; and references therein), in order to derive its abundance of Bi and other neutron-capture elements.

2. OBSERVATIONS, REDUCTIONS, AND ANALYSIS

Spectra of CS29497-030 were obtained 2004 September 29–October 1 with the blue configuration of the Keck I High Resolution Echelle Spectrometer (HIRESb; Vogt et al. 1994) and new 3-chip CCD mosaic ($3 \times 2048 \times 4096 \times 15 \mu\text{m}$ pixels). The wavelength range coverage is essentially continuous in the range $\sim 3050\text{--}5895 \text{ \AA}$. With 3×1 pixel on-chip binning and a slit width of 0.861 arcseconds, we obtained resolving power $R \equiv \lambda/\Delta\lambda \simeq 40,000$. Nine 1800 s exposures were taken to attain a co-added signal-to-noise ratio (S/N) of 55:1 per resolution element in the centre of the blaze of the bluest order. The S/N increases redwards, with ~ 100 at $\lambda 3680 \text{ \AA}$, ~ 250 at $\lambda 4400 \text{ \AA}$, and ~ 300 at $\lambda 5850 \text{ \AA}$. Data reduction was performed using standard tasks in IRAF⁸, FIGARO⁹, and SPECTRE (Fitzpatrick & Sneden 1987).

Our abundance analysis relied on the results of a combination of spectrum syntheses and equivalent width (EW) analyses measured with SPECTRE by fitting Gaussian profiles to the absorption lines. We employed stellar atmospheres without overshooting (Castelli & Kurucz 2004), and performed abundance calculations with a current version of MOOG (Snedden 1973). Adopting the stellar parameters of SPC03 as initial parameters, we then iterated on the Fe abundances to eliminate abundance trends with respect to the excitation potentials, EWs, and ionization states. We derive values of $T_{\text{eff}} = 7000 \text{ K}$, $\log g = 4.1$, $\xi_t = 1.9 \text{ km s}^{-1}$, and $[\text{Fe}/\text{H}] = -2.57$, all in good agreement with SPC03, with the exception of the lower metallicity derived from the higher quality data employed in this study. We also compared our abundances for CS29497-030 to those of Sivarani et al. (2004). With 19 elements in common between the two studies (excluding those for which only an upper limit was derived), most of the abundances agree to within $1\text{-}\sigma$. Abundances in largest disagreement can be completely explained as the direct result of the differences in the adopted stellar parameters. As Sivarani et al. show (their Table 2), the photometry of CS29497-030 leads to a wide range of T_{eff} values based on colours. In this study, we adopt the value of 7000 K, which satisfies both our spectroscopic constraints and is comparable to

the estimate based on ($V\text{--}K$) photometry. Further technical details regarding our reduction and analysis techniques will be reported in an expanded investigation currently underway (Ivans et al. 2005).

In Figure 1 we illustrate three 4\AA -swaths of spectrum syntheses surrounding regions of selected near-UV features of platinum, bismuth, lead, erbium, and ytterbium. In Table 1 we list our abundances for CS29497-030, including formal uncertainties of their means (\pm), and the adopted $1\text{-}\sigma$, which includes an allowance for any uncertainty in the spectroscopically derived stellar parameters. Abundances derived from a single feature have been assigned $\sigma = 0.3$ dex. For some elements with additional useful features at wavelengths redward of our HIRESb set-up, we made new abundance determinations of the 2D-FRUTTI data employed by SPC03.

The derived abundances of O, Na, Al, and K shown in Table 1 have not been corrected for non-local thermodynamic equilibrium (NLTE) effects which are known to exist for these elements. The available literature on this issue in *warm* low metallicity stars is both sparse and in poor agreement. For the elemental abundances of O, Na, Al, and K, we suggest that the following values be considered with greater confidence: upper limits of $[\text{O}/\text{Fe}] \leq +1.59$; $[\text{Na}/\text{Fe}] \leq +0.88$; $[\text{Al}/\text{Fe}] \leq +0.58$; and $[\text{K}/\text{Fe}] \leq +1.07$; which include our estimated NLTE corrections.

3. DISCUSSION

We explored the origin of the neutron-capture elements in CS29497-030 by comparing the observed abundances with predicted r - and s -process contributions. In Figure 2, we display our abundances in the context of s -process FRANEC calculations performed by Gallino et al. (1998, 2005; also see Straniero et al. 2005; and references therein). Predictions from two sets of initial abundance assumptions are shown: with and without pre-enrichment of the initial abundances. [La/Eu] ratios produced in the s -process at this low metallicity are typically $+0.7$ dex. In CS29497-030 the [La/Eu] ratio is ~ 0.2 , clearly indicating a strong r -process contribution. The pre-enrichment treatment employed in the s -process calculations here permits an exploration of the possibility that the initial abundances of CS29497-030 and its binary partner arose from a parent cloud with an extreme r -process abundance. In our picture, the formation of this pair of low mass stars was triggered by a supernova which polluted, snowplowed, and clumped a nearby molecular cloud. In the associated s -process calculation, all of the initial r -process isotopes have been enhanced (according to their r -process contribution to the solar system abundances and normalized to Eu) and this, in turn, affects the seed abundances available to the subsequent s -processing.

In the case of no pre-enrichment, the displayed result represents the most recent FRANEC calculations of the s -process at $[\text{Fe}/\text{H}] \sim -2.6$ for an AGB star of $1.3M_{\odot}$ with an enhanced ^{13}C abundance, in which all heavy-element abundance predictions are from the s -process. Also illustrated in Figure 2 are s -process calculations based on the r -process pre-enrichment scenario. Calculations for $\pm 0.05M_{\odot}$ produce abundances which bracket those shown in the figure.

The main component of the s -process is produced in an AGB star undergoing a series of He shell flashes via

⁸ IRAF is distributed by NOAO, which is operated by AURA, under cooperative agreement with the NSF.

⁹ FIGARO is provided by the Starlink Project which is run by CCLRC on behalf of PPARC (UK).

the triple- α reaction just below the H-burning shell. In these He-shell flashes (pulses), proton mixing leads to $^{12}\text{C}(p,\gamma)^{13}\text{N}(e^+, \nu)^{13}\text{C}(\alpha, n)^{16}\text{O}$ reactions, releasing neutrons which can then be captured by Fe and heavy-element seeds (Iben & Renzini 1982; Busso et al. 1999; Straniero et al. 2005). The next thermal pulse injects the energy required to dredge up the nucleosynthesis products into the envelope while mixing more protons with the products of further triple- α reactions. Thus, the photospheric abundance ratios of neutron-rich elements created in the s -process are a function of the histories of the envelope and core masses, and the number of thermal pulses.

The number of thermal pulses affects the number of free neutrons for subsequent neutron-capture processing and the abundance of Na places a stringent limit upon the assumed AGB star progenitor mass. The Na abundance results from $^{22}\text{Ne}(n,\gamma)^{23}\text{Na}$ reactions where ^{22}Ne is largely of primary origin, only slightly affected by α -captures during the thermal pulses. ^{22}Ne derives its abundance from CNO nuclei ashes (^{14}N) capturing α -particles in the convective thermal pulse, with primary ^{12}C produced and mixed to the surface by previous dredge-up episodes. More massive AGB models produce higher [Na/Fe] abundances (e.g., $1.5M_{\odot}$ model undergoes ~ 20 thermal pulses \Rightarrow [Na/Fe] ~ 2). The best fit to our recommended upper limit of [Na/Fe], as well as the overall abundances of CS29497-030, was found to be from a $1.3M_{\odot}$ AGB model that had undergone only six thermal pulses.

Among the light neutron-capture elements, where no r -process enrichment was assumed, the s -process model with pre-enrichment predicts abundances in good agreement with those derived for Sr and Zr. An “intrinsic AGB” (i.e., high luminosity and low $\log g$) is expected to be Tc-rich, ^{93}Zr -rich, and ^{93}Nb -poor (Wallerstein & Dominy 1988). An “extrinsic AGB” is on or near the main sequence, and was once the smaller mass star in a binary system. The s -process abundances of the extrinsic AGB star are a result of pollution from the former AGB star’s dredged-up material, at an epoch sufficiently remote for the ^{93}Zr to have now decayed to ^{93}Nb . Our [Nb/Zr] ratio and stellar parameters for CS29497-030 are both in accord with those of an extrinsic AGB.

The abundances of elements in CS29497-030 with large s -process contributions in the solar system are predicted to have lower abundances in the $r+s$ results than those predicted from the s -process operating without r -process pre-enrichment. The pre-enrichment of the additional heavy elements affects the s -processing within the He-intershell of the AGB star, both in the ^{13}C -pocket and the convective thermal pulse. Because the heavy element isotopes in the pre-enrichment case are so numerous, they strongly compete with Fe as seeds for neutron-capture. In addition, this competition takes a global role of leaving fewer neutrons available for the s -process isotopes which further decreases s -process efficiency.

Other $r+s$ stars have recently been reported and discussed in the literature (e.g. Aoki et al. 2002; Cohen et al. 2003; Johnson & Bolte 2004; Zijlstra 2004; Barbay et al. 2005 and references therein). In some of the previous efforts to model the abundances of $r+s$ stars, s -process material has been added to existing r -

process abundance enhancements (e.g., Delaude 2004). However, those modelling attempts were performed employing fewer abundances than those employed here for CS29497-030, and the previous attempts neither required nor included s -processing of the r -enhanced material within the He-intershell of the AGB star as has been done in the present study. As noted, CS29497-030 possesses the largest [Pb/Fe] abundance of any metal-poor star published to date. Its s -process contribution to Bi disguises its initial r -process contribution. However, we predict that $r+s$ stars with *less* s -processing (and a relatively higher amount of r -processed material) will provide 3rd s -peak abundance ratios which can then be used to pin down the abundance predictions – and production sites – for the production of the r -process actinide elements such as Th and U.

4. CONCLUSIONS

The chemical abundances of the extremely Pb-rich BMP star CS29497-030 are an excellent testbed to set new constraints on models of neutron-capture processes at low metallicity. We find CS29497-030 to be an $r+s$ star and that the abundance ratios are best fit by a pre-enrichment of r -process material out of which the binary system formed. The more massive companion underwent an AGB phase, and heavy elements from the pre-enrichment competed with Fe as seeds for neutron-capture, leaving fewer neutrons available for s -process isotopes, diminishing the s -process efficiency. Pollution from the former AGB star’s dredged-up material subsequently enriched the envelope composition of CS29497-030. Based on the fit to the low number of AGB model thermal pulses to match the observed abundance pattern, including the abundances of Na and Mg, we deduce that the progenitor mass of the AGB star was $1.3M_{\odot}$. The relative abundances we derive for Nb and Zr, as well as the stellar parameters corresponding to an evolutionary stage near the main sequence, confirm that CS29497-030 is an extrinsic AGB star.

We encourage future studies of s -process abundance patterns to include the abundance of light elements sensitive to the neutron excess such as Na and Mg. We find that these elements are useful constraints on the mass of the AGB progenitor. However, some light elements are affected by NLTE effects and studies to date of those effects are sparse and/or in poor agreement. It would be useful to extend the knowledge to lower metallicity and warmer temperatures than have so far been investigated.

Overall, the predicted abundances from the $r+s$ -process fit well the observed abundance patterns of CS29497-030, from the first- (Sr and Zr) and second-peaks of the s -process (Ba and La) as well as the third-peak (Pb and Bi). Our abundance determination for Bi is the first such in any metal-poor star. And, the value derived for Bi is in accord with the Pb abundance. We find that the s -process contribution to the pre-enrichment of r -process material in CS29497-030 swamps the r -process signature in the abundance of Bi. We recommend that additional $r+s$ stars (but with relatively less s -processing than is found in CS29497-030) be observed in order to derive Pb and Bi abundances that may further illuminate the issues regarding the production of actinide elements, Th and U and the other neutron-capture processes at work at early times in our Galaxy.

We thank the following agencies for providing funding support for this research: NASA through Hubble Fellowship grant HST-HF-01151.01-A from the Space Telescope Science Inst., operated by AURA, under NASA contract NAS5-26555 to III; NSF through grants AST03-07495 to CS and AST03-07279 to JJC; and MIUR-FIRB (Italy) “The astrophysical origin of heavy elements beyond Fe” to RG. We are also grateful for the privilege

of conducting observations from the revered summit of Mauna Kea. We also acknowledge and appreciate the use of NASA’s Astrophysics Data System Bibliographic Services; the successful efforts by the HIRES CCD upgrade group; the knowledgeable expertise of Keck staff during the run; and the generous help and patience of Sara Bisterzo in the generation of the FRANEC models.

REFERENCES

- Aoki, W., Ryan, S. G., Norris, J. E., Beers, T. C., Ando, H., & Tsangarides, S. 2002, *ApJ*, 580, 1149
- Arlandini, C., Käppeler, F., Wisshak, K., Gallino, R., Lugaro, M., Maurizio B., & Straniero, O. 1999, *ApJ*, 525, 886
- Barbuy, B., Spite, M., Spite, F., Hill, V., Cayrel, R., Plez, B., & Petitjean, P. 2005, *A&A*, 429, 1031
- Burris, D. L., Pilachowski, C. A., Armandroff, T. A., Sneden, C., Cowan, J. J., & Roe, H. 2000, *ApJ*, 544, 302
- Busso, M., Gallino, R., & Wasserburg, G., J. 1999, *ARA&A*, 37, 239
- Castelli, F., & Kurucz, R. L. 2003, *Modelling of Stellar Atmospheres*, N. E. Piskunov, W. W. Weiss, D. F. Gray, *ASP*, 210, 20
- Clayton, D., D., & Rassbach, M. E. 1967, *ApJ*, 148, 69
- Cohen, J. G., Christlieb, N., Qian, Y.-Z., & Wasserburg, G. J. 2003, *AJ*, 588, 1082
- Delaude, D., Gallino, R., Cristallo, S., Straniero, O., Husti, L., & Ryan, S. 2004, *Mem. S. A. It.*, 75, 706
- Fitzpatrick, M. J., & Sneden, C. 1987, *BAAS*, 19, 1129
- Gallino, R., Arlandini, C., Busso, M., Lugaro, M., Travaglio, C., Straniero, O., Chieffi, A. & Limongi, M. 1998, *ApJ*, 497, 388
- Gallino, R., et al. 2005, in preparation
- Iben, Jr. I., & Renzini, R. 1982, *ApJ*, 263, L23
- Ivans, I. I., et al. 2005, in preparation
- Johnson, J. A. & Bolte, M. 2004, *ApJ*, 605, 462
- Kratz, K.-L., Pfeiffer, B., Cowan, J. J., & Sneden, C. 2003, *New Ast. Rev.*, 204, 105
- Preston, G. W., Beers, T. C., & Schectman, S. A. 1994, *AJ*, 108, 538
- Ratzel, U., Arlandini, C., Käppeler, F., Couture, A., Wiescher, M., Reifarth, R., Gallino, R., Mengoni, A., & Travaglio, C. 2004, *Phys. Rev. C*, 70, 065803
- Simmerer, J., Sneden, C., Cowan, J. J., Collier, J., Woolf, V. M., Lawler, J. E. 2004, *ApJ*, 617, 1091
- Sivarani, T., Bonifacio, P., Molaro, P., Cayrel, R., Spite, M., Spite, F., Plez, B., Andersen, J. et al. 2004, *A&A*, 413, 1073
- Sneden, C. 1973, *ApJ*, 184, 839
- Sneden, C., Preston, G. W., & Cowan, J. J. 2003, *ApJ*, 592, 504 [SPC03]
- Straniero, O., Gallino, R., & Cristallo, S. 2005, submitted, *Nuclear Physics A*
- Takeda, Y., Zhao, G., Chen, Y.-Q., Qiu, H.-M., & Takada-Hidai, M. 2002, *PASJ*, 54, 275
- Travaglio, C., Galli, D., Gallino, R., Busso, M., Ferrini, F. & Straniero, O. 1999, *ApJ*, 521, 691
- Van Eck, S., Goriely, S., Jorissen, A., & Plez, B. 2003, *A&A*, 404, 291
- Vogt, S. S., Allen, S. L., Bigelow, B. C., Bresee, L., Brown, B., Cantrall, T., Conrad, A., Couture, M., et al. 1994, *SPIE*, 2198, 362
- Wallerstein, G., & Dominy, J. F. 1988, *ApJ*, 330, 937
- Zijlstra, A. A. 2004, *MNRAS*, 348, L23

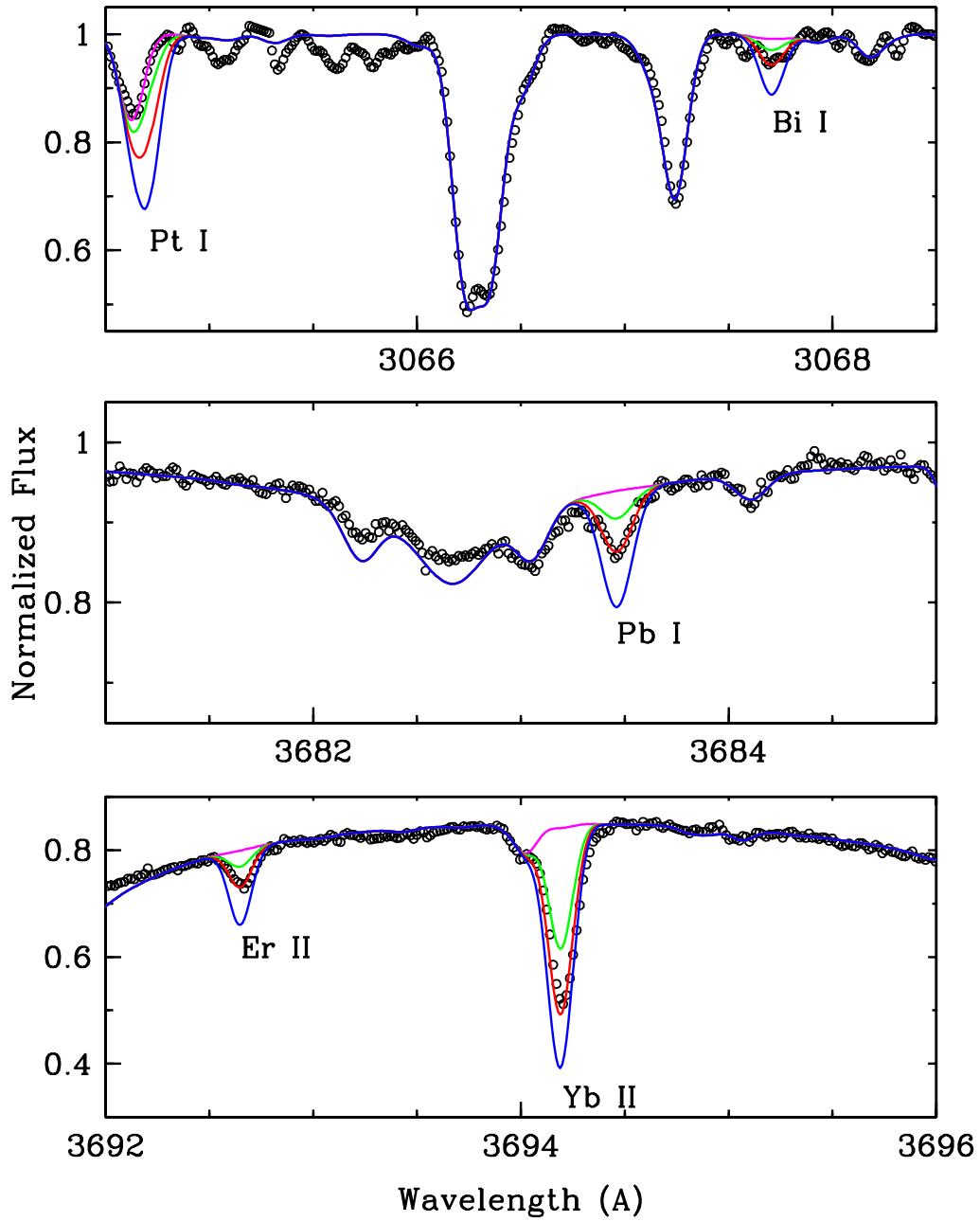


FIG. 1.— Spectra surrounding platinum, bismuth, lead, erbium, and ytterbium features in the near-UV. The dots represent the observed spectrum and the solid lines, the spectrum syntheses. The magenta line represents a synthesis with no detectable contribution of the named element (e.g., only an upper limit is derived for platinum). The green and blue syntheses otherwise bracket the derived abundances (presented in Table 1 and displayed here in red) by ± 0.4 dex.

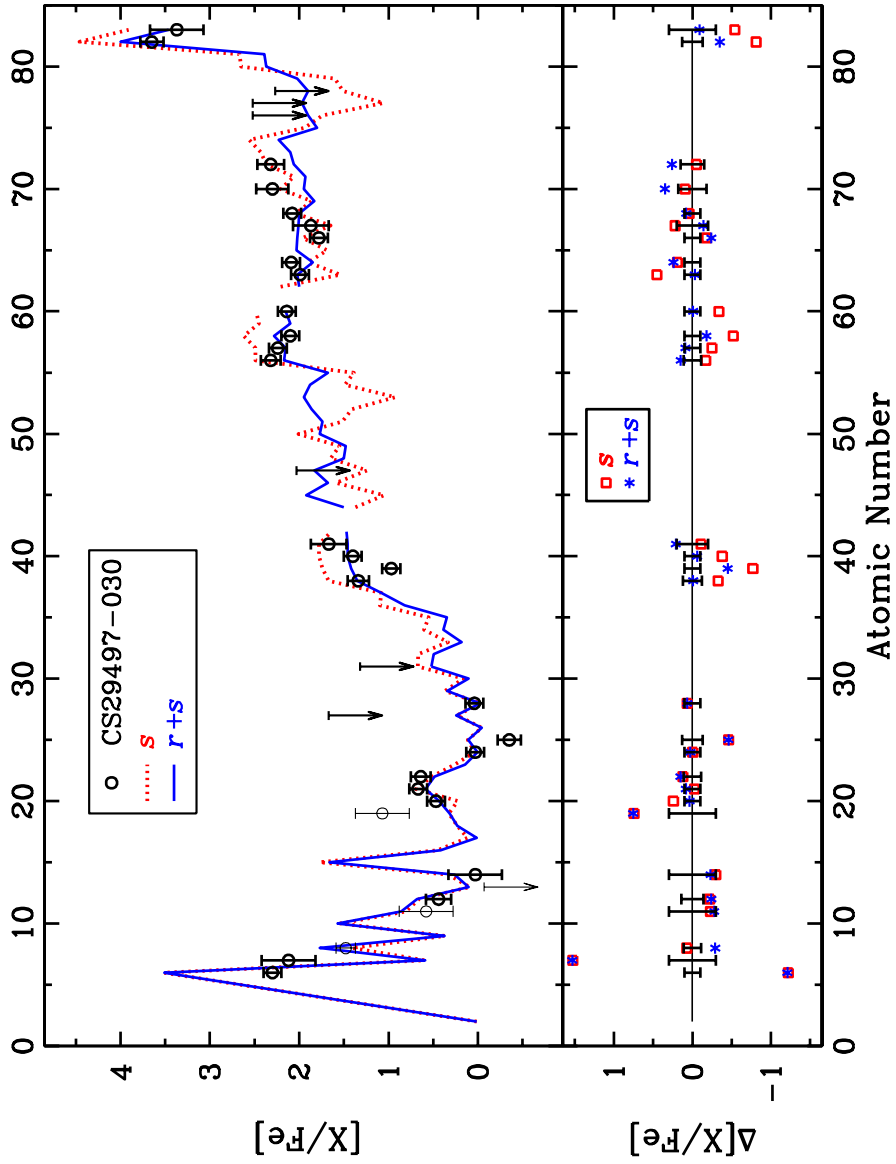


FIG. 2.— Comparison of the $[X/Fe]$ abundances in CS29497-030 with predictions from s -process calculations of a $1.3M_{\odot}$ AGB star model. In the top panel, the upper limits and open circles with error bars denote the stellar abundances. Thinned symbols denote the four light element abundances which may suffer from uncorrected NLTE systematics (see § 2). The solid blue line represents the best fit s -process calculations based on an extreme r -process abundance pre-enrichment ($r+s$); the red dotted line represents predictions from s -process calculations without r -process enrichment. The bottom panel displays the difference defined as $\Delta[X/Fe] \equiv [Fe/H]_{\text{obs}} - [Fe/H]_{\text{calc}}$ and upper limits are not shown.

TABLE 1
CS29497-030: DERIVED ABUNDANCES

Species	Element	$\log \epsilon(X)$	\pm	n	[X/Fe]	σ
C	6	8.29	0.03	9	+2.30	0.10
C (CH)	6	8.46	+2.47	0.10
N (CN)	7	7.60	+2.12	0.35
O ^(a)	8	7.84	0.11	3	+1.48	0.11
Na ^(a)	11	4.34	...	1	+0.58	0.30
Mg	12	5.45	0.07	4	+0.44	0.14
Si	14	5.01	...	1	+0.03	0.30
K ^(a)	19	3.62	...	1	+1.07	0.30
Ca	20	4.26	0.04	6	+0.47	0.10
Sc	21	1.20	0.01	3	+0.67	0.10
Ti	22	3.06	0.03	17	+0.64	0.11
Cr	24	3.13	0.04	5	+0.03	0.10
Mn	25	2.47	0.07	4	-0.35	0.13
Ni	28	3.72	0.02	2	+0.04	0.10
Sr	38	1.67	0.07	3	+1.34	0.12
Y	39	0.64	0.02	13	+0.97	0.10
Zr	40	1.43	0.03	11	+1.40	0.10
Nb	41	0.52	0.04	3	+1.67	0.20
Ba	56	1.88	0.06	3	+2.32	0.11
La	57	0.80	0.01	15	+2.22	0.10
Ce	58	1.08	0.02	20	+2.10	0.10
Nd	60	1.02	0.02	17	+2.14	0.10
Eu	63	-0.07	0.03	6	+1.99	0.10
Gd	64	0.64	0.02	5	+2.09	0.10
Dy	66	0.31	0.02	7	+1.78	0.10
Ho	67	-0.19	0.05	4	+1.87	0.20
Er	68	0.44	0.04	4	+2.08	0.10
Yb	70	0.81	0.13	2	+2.30	0.18
Hf	72	0.63	0.07	5	+2.32	0.15
Pb	82	2.93	0.07	3	+3.65	0.13
Bi	83	1.51	...	1	+3.37	0.30
Upper Limits						
Al ^(a)	13	3.83	...	1	-0.07	...
Co	24	4.02	...	1	+1.67	...
Ga	31	1.63	...	1	+1.32	...
Ag	47	0.7:	...	1	+2.03	...
Os	76	1.4:	...	1	+2.52	...
Ir	77	1.3:	...	1	+2.52	...
Pt	78	1.5:	...	1	+2.27	...

^(a)Derived abundance does not take into account NLTE correction which would revise abundance. See § 2 for discussion and recommended upper limits.